Oscillatory and chaotic regimes of patterns and dark cavity solitons in cavities displaying EIT: static multihead dual chimera states

Mansour Eslami[1],* Maryam Kanafchian[1], and Gian-Luca Oppo[2]

[1]*Department of Physics, University of Guilan, P.O. Box 41335-1914 Rasht, Iran*

[2]*SUPA and Department of Physics,*

University of Strathclyde, Glasgow, G4 0NG, Scotland, UK

This is a peer-reviewed, accepted author manuscript of the following article: Eslami, M., Kanafchian, M., & Oppo, G-L. (2023). Oscillatory and chaotic regimes of patterns and dark cavity solitons in cavities displaying EIT: static multihead dual chimera states. Chaos, Solitons and Fractals, 167, [113080]. https://doi.org/10.1016/j.chaos.2022.113080

Abstract

Oscillating and chaotic regimes of honeycomb patterns and dark cavity solitons are studied in a cavity displaying electromagnetically induced transparency. Considering a three-level atomic system in Λ configuration, transition to chaotically oscillating honeycombs is numerically investigated and their dynamical behavior is detailed in different control parameter values. We show that a branch of oscillating dark cavity solitons coexists with the honeycomb patterns. These oscillating cavity solitons are studied individually and in mutual interaction. In particular, it is shown that mutually coherent oscillating dark cavity solitons can be obtained by choosing an appropriate separation distance. Finally, we introduce a novel regime of chimera states consisting of multitude of identically and non-locally coupled dark cavity solitons in which regions of in-phase and anti-phase coherence separated by incoherent areas coexist and are stationary. We discuss the unique features of these structures and categorize them as static multihead dual chimera state. We believe that this is for the first time that such chimeric states are reported in a photonic system hosing oscillating and chaotic structures.

I. INTRODUCTION

Nonlinear spatially extended systems can form a variety of spatiotemporal structures from regular patterns to disordered, chaotic and turbulent structures in different scientific disciplines [1–3]. In nonlinear optics, these have supplemented with localized solutions such as propagation solitons, cavity solitons (CSs), light bullets (LBs) and even optical rogue waves (RWs) [4, 5]. In optical cavities, spatial coupling through diffraction or dispersion accommodates the system with a large number of transverse or longitudinal spatial modes whose presence and interactions are the source of interesting dynamical behaviors. The nonlinear nature of these interactions results in instabilities and bifurcations which can lead to self-pulsing and excitable dynamics [6–9] as well as extended turbulence with possible generation of 2D RWs, optical vortices, and spatio-temporal chaos [10–17]. After the early observations of regular and stationary patterns and localized structures, the introduction of oscillatory patterns and their analysis via secondary bifurcations paved the way for understanding the possible routes for chaos and symmetry breaking mechanisms [18–20]. It has

* meslami@guilan.ac.ir

been reported in [19] that the interplay between spatial and temporal degrees of freedom leads to a series of bifurcations showing spatial-period multiplying and quasi-periodicity for hexagonal optical patterns. It has also been shown that spatial order is completely lost through series of instabilities which cause the system to enter a regime of optical turbulence. In another study in the same system, a Kerr cavity with self-focusing nonlinearity pumped by an external field, they have found strong correlation between intensity fluctuations of any arbitrary pair of wave vectors of the pattern [18].

To date, not much work has been done about the dynamics of CSs in oscillatory and chaotic regimes. Bright (dark) CSs are isolated intensity peaks (dips) sitting on a homogeneous low (high) intensity background and play a key role in photonic devices that are at the base of novel technologies such as all-optical information bits, switches and frequency combs [21–34]. Dynamical regimes of CSs, e.g. oscillatory and chaotic, are therefore important from both the fundamental and the application point of view. These topics have been covered in a variety of broad-area systems from driven nonlinear optical cavities to configurations of vertical-cavity surface-emitting lasers (VCSELs) and cavities displaying quantum coherent phenomena in [6, 35–41].

Collective behavior of oscillating CSs is also an important topic of investigation due to their emergent properties. For example, it has been shown in [37] that the transition from stationary to oscillating CSs can lead to an enhancement of the soliton interaction strength. Mutually interacting oscillating CSs have been shown to exhibit regimes of synchronized, anti-synchronized (or anti-phase synchronization) and de-synchronized dynamics with interesting consequences in terms of mutual correlation and coherence [42, 43]. Moreover, while coupled non-identical oscillators have long been known to exhibit complex dynamical phenomena like frequency and phase locking, partial synchronization and complete incoherence, coupled identical oscillators were believed to either synchronize in phase or to remain incoherent indefinitely [44]. Observation of coexisting regions of coherent (phase and frequency locked) and incoherent (drifting) oscillations by Kuramoto and Battogtokh when all of the oscillators were identical surprised, however, many researchers in the nonlinear dynamics community and excited numerous research topics [45–47]. Among them are the so-called chimera states, spatiotemporal patterns in which a system of identical oscillators is split into coexisting regions of coherent and incoherent oscillations. In other words, some of the oscillators synchronize while others remain incoherent. At the time of its discovery,

this behavior was at odds with the common belief that moving from complete incoherence to (partial) coherence required changes of coupling strengths. Their coexistence in chimera states could only be attributed to the heterogeneities in the natural frequencies [47].

Over the years, a wide variety of chimeric features have been reported with new definitions and classifications (see [48] and references therein). Different features of chimera states are specific to certain types of models due to the different type of oscillators, initial conditions [49], geometries, and coupling. The latter can include discrete dissipative coupled systems as, for example, reported in [50]. **For a useful list of systems where chimeras have been analysed in a variety of different topological settings, i.e. different geometries and/or coupling functions, see the Appendix of Ref. [47].** Some chimera features, such as simultaneous presence of in-phase and anti-phase order, their multiplicity, separation by disorder, and persistence were thought to be impossible to be displayed by a single physical system [48, 51]. Therefore, observation of a state with a collection of chimeric features in a single physical system can paint a different and interesting picture. Here we report a first study (to the best of our knowledge) of 1D and 2D chimera states in a nonlinear optical cavity hosting interacting oscillating cavity solitons, which is a hybrid of different specifications listed above.

We consider here a 3-level medium in a cavity capable of displaying electromagnetically induced transparency (EIT) via multi-level quantum interference. In this system, we study oscillating and chaotic regimes of extended patterns and CSs. This model has already been shown to support multistability of patterns and CSs, extended optical turbulence and RWs in 2D diffractive regimes [10, 41, 52–54] and, more recently, domain walls, temporal CSs and even cavity Stimulated Raman adiabatic passage (STIRAP) with no input pulses [34]. In particular, temporal CSs can lead to frequency combs in 1D dispersive regime via quantum interference [34]. In this contribution we focus on the transition dynamics from homogeneous state to stable honeycombs (HC) and to chaotic HC patterns. Formation of dark cavity solitons (DCSs) in an appropriate parameter region is also studied and their oscillating dynamics are investigated in different control parameter values. We also investigate the interaction of two DCSs in the oscillating regime where mutual correlations and coherence are parameter dependent. We report a novel regime of static multihead dual chimera state where non-locally coupled oscillating DCSs form clusters of in-phase and anti-phase coherent states (phase locked) that remain separated by incoherent (phase unlocked) regions.

Details of the three-level cavity model appear in section 2, the dynamical properties of oscillating and chaotic HC patterns are discussed in section 3 and those of DCSs and their interaction in section 4. Coupled DCSs forming chimera states are discussed in section 5. Conclusions and final remarks are contained in Section 6.

II. THE MODEL

We consider a ring cavity, Fig. 1(a), filled with three-level atoms in Λ configuration, Fig. 1(b), under the action of two pump beams fulfilling the conditions for coherent population trapping (CPT) and EIT [34, 52–54]. In a Λ atomic configuration we consider three separate energy levels, the ground state $|1>$, a long lived intermediate ground state $|2>$, and an excited state $|3>$ with $|1>$ and $|2>$ of same parity so that the transition $|1>\Leftrightarrow|2>$ is not dipole allowed. Two laser beams of frequencies close to the atomic frequencies of the $|1>\Leftrightarrow|3>$ and $|2>\Leftrightarrow|3>$ transitions complete the Λ scheme as displayed in Fig. 1(b). A pump beam of real amplitude P and detuned by $\Delta=-0.2$ from the $|1>\Leftrightarrow|3>$ transition (red detuned case) is injected into the cavity. This pump beam P is also mistuned from the cavity resonance frequency by $\theta=-1$ while the second field, E_2, referred to as the coupling field in EIT literature, is at resonance with the $|2>\Leftrightarrow|3>$ transition and is not resonated in the cavity. The mean field equation for a beam propagating in such a cavity is [52]:

$$\partial_t E = P - (1+i\theta)E + 2iC\rho_{13} + i\nabla^2 E \tag{1}$$

$$\rho_{13} = \chi E = -\frac{\Delta|E_2|^2\left(|E_2|^2+|E|^2-i\Delta\right)}{\left(|E_2|^2+|E|^2\right)^3}\,E\,, \tag{2}$$

where ρ_{13} is the off-diagonal density matrix element which is proportional to the field amplitude E via Eq. 2 obtained under the condition of $\Delta^2 \ll |E_2|^2$. The real (dispersion) and imaginary (absorption) parts of the susceptibility χ are shown in Fig. 2(a) in terms of the material detuning where the vanishing absorption close to the medium resonance clearly evidences the EIT phenomenon. $2C$ is the co-operative parameter directly proportional to the atomic density n_a, the square of the dipole moment of the given transition μ^2, the wave

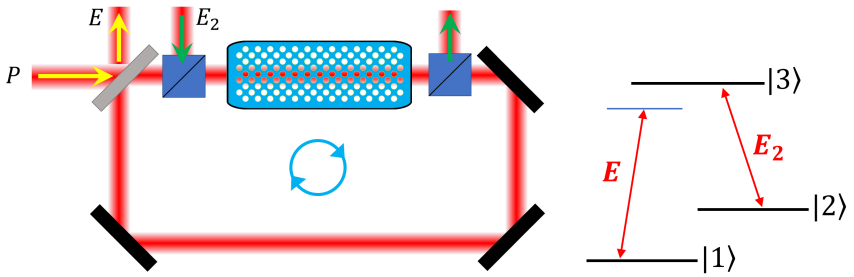

FIG. 1. (a) The cavity configuration under the action of the pump P and coupling E_2 fields. **(b) The Λ atomic scheme with two ground states $|1>, |2>$, a single excited level $|3>$ and two laser beams (red arrows). Note that in experiments where atomic ground states and optical fields have small frequency differences (few GHz), polarizing beam splitters are used so that the coupling beam E_2 is not resonated in the cavity. BS, PBS, and M stand for beam splitter, polarizing beam splitter and mirror, respectively.**

number k of the field E and the length of the cavity L, being inversely proportional to the reduced Planck constant $\hbar$, the atomic linewidth $\gamma_\perp$ and permittivity of free space ϵ_0 normalized by the cavity transmittivity T

$$2C = (n_a \mu^2 k L)/(2\hbar\gamma_\perp \epsilon_0 T) \ . \tag{3}$$

Both $2C$ and P are considered as the control parameters in our simulations. Diffraction is described by the Laplacian operator ∇^2 in two transverse dimensions (X **and** Y)and time is normalized to the photon lifetime. Details of the derivation of the diffractive and dispersive Maxwell-Bloch Eq. 1 for the case of a two-level medium are provided in [34, 52, 55, 56]. The split-step method is adopted for the simulation of the system and consists of a Runge-Kutta algorithm for the time evolution and Fast Fourier Transform (FFT) for dealing with the diffraction term. We consider transverse domains of side w (typically in the range of $0.1-10$ mm). Depending on the structure under study, we have used $N \times N$ grid points with $N = 64, 128, 256, 512$ and same size w. In order to ensure proper stability and convergence of the algorithm, time step of 10^{-3} and transverse size of $10\lambda_c$ in normalized units have been used where $\lambda_c = 2\pi/k_c$ with k_c being the critical wave vector of $\sqrt{-\theta}$ as used in [53]. Bistability of the homogeneous stationary solutions (HSS) and multistability of the spatial structures have already been shown for a saturable Kerr case and the generalized model close to EIT respectively in [52] and [53, 54]. In this paper, we consider parameter values

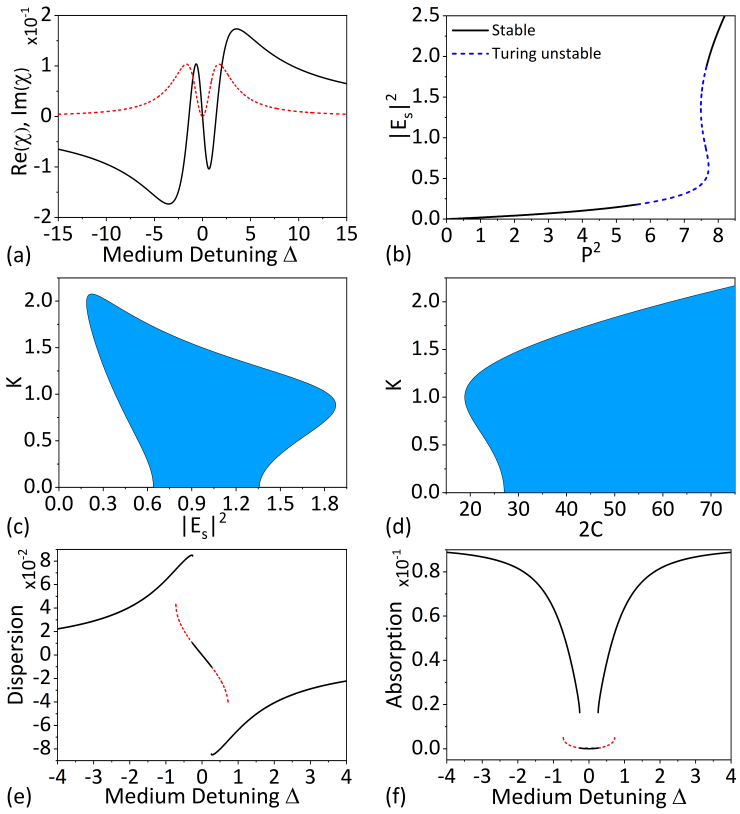

FIG. 2. (a) The imaginary (red dashed) and real (black solid) parts of the complex susceptibility χ **(Eq. 2) for** $|E_s|^2 = |E_2|^2 = 1$**. (b) Intensity input/output diagram** and (c) Turing instability domain responsible for pattern formation for fixed values of $\Delta = -0.2$, $\theta = -1$, $2C = 30$, and $|E_2|^2 = 1$. (d) Map of (c) on the $2C - K$ space (K being the transverse wavevector) for $|E_s|^2 = 1$. (e) Chromatic dispersion $\mathrm{Re}(\rho_{13})$ and (f) absorption $\mathrm{Im}(\rho_{13})$ versus the material detuning Δ for the $|1> \Leftrightarrow |3>$ transition for $\theta = 0, |E_2|^2 = 1$, and $P = 2.75$. Solid black (red dashed) corresponds to low (high) intensity branch of the bistable HSS.

leading to red-detuned nonlinearity where HCs and DCSs are expected to form. **It is possible to perform a linear stability analysis of the homogeneous steady states where the second derivative term becomes a linear term in the magnitude square of the transverse wavevector K. By determining the eigenvalues with zero or positive real parts via a characteristic equation, unstable transverse wavevectors are obtained. These wavevectors rule the periodicity of the incoming pattern in a mechanism typical of Turing pattern formation [1, 55, 57]. In conservative systems like the nonlinear Schrödinger equation, similar instabilities have been**

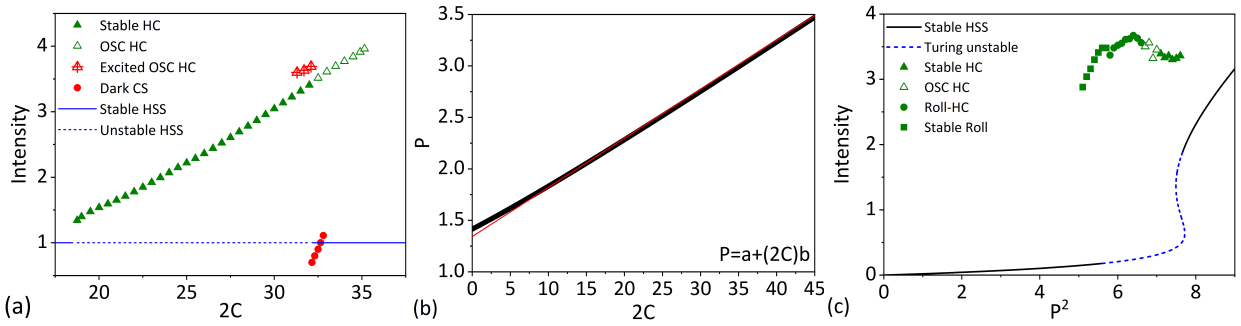

FIG. 3. (a) Intensities of spatio-temporal structures in a $2C$ scan when keeping the HSS intensity fixed at the value 1 (horizontal line, dashed for Turing unstable and solid for stable parts). Stable (oscillating) HCs correspond to filled (empty) triangles resulting from the adiabatic increase of the control parameters starting from below the Turing threshold. Intensity minima of dark cavity solitons correspond to filled circles. (b) Values of P versus $2C$ when keeping the HSS intensity fixed at the value 1 as in (a). The linear fit $P = a + (2C)b$ provides $a = 1.34$ and $b = 0.047$. (c) Branches of solutions versus P^2 obtained by an adiabatic scan of the pump intensity for fixed $2C = 30$. We note that this value of $2C$ does not support DCSs. For the cases of oscillating/chaotic HCs the mean value of intensities is considered. **HC and OSC stand for the terms "honeycomb" and "oscillating", respectively.** For other parameter values see Fig. 2.

called modulational instabilities. Our complex equation 1 is, however, dissipative and the presence of diffraction makes it mathematically equivalent to typical Turing diffusive systems as demonstrated in [57].

We show in Fig. 2(b)-(d), the **intensity input/output diagram** along with the Turing instability domains **(where at least one linear stability eigenvalue with wavevector K different from zero is positive)** with respect to both the stationary intensity $|E_s|^2$ and $2C$. It is seen that the lower intensity branch of the **input/output diagram** is affected by the Turing instability which confirms the possibility of DCS formation. In Fig. 2(e) and (f) we show the chromatic dispersion and absorption properties of the transition $|1> \Leftrightarrow |3>$ of the Λ system for the two bistable HSS at cavity resonance when changing Δ. In [10, 41, 53, 54] we have shown that the system is extremely sensitive to different values of the control parameter with several and distinct bifurcations that lead to different sets of possible solutions. For the regime considered here, sensitivity to parameter values and initial conditions results in having two branches of solutions in the Turing unstable region

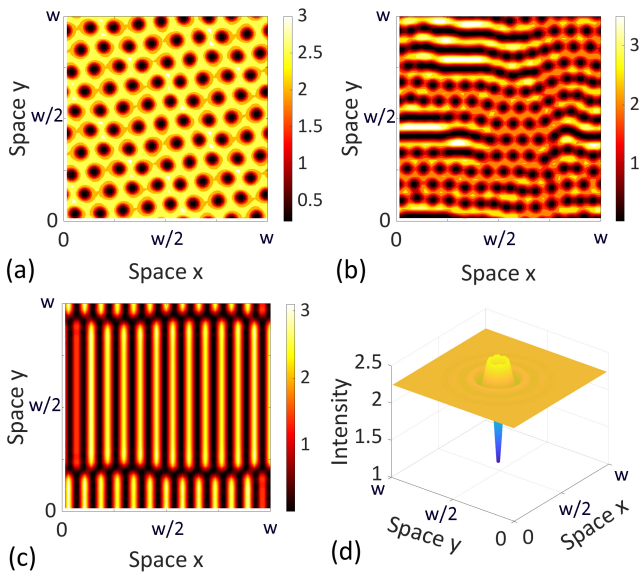

FIG. 4. Snapshots from **numerical simulations of Eq. 1 along the solution** branches shown in Fig. 3. (a) Honeycomb pattern for $2C = 31.5$ and $P^2 = 7.70$, (b) bistable roll-honeycomb structure for $2C = 31.5$ and $P^2 = 6.60$, (c) roll pattern for $2C = 31.5$ and $P^2 = 5.20$ and (d) oscillating dark cavity soliton for $2C = 32.8$ and $P^2 = 8.32$.

with distinct properties. By choosing the initial value of the control parameter $2C$ less than the bifurcation point ($2C = 18.8$) and adiabatically following the increase of $2C$ value, it is possible to catch a secondary bifurcation point at $2C = 32.50$ beyond which a stable HC pattern starts to oscillate and eventually we achieve a regime of chaotic HC. However, by choosing the initial value of the control parameter in the Turing interval and starting from noise a branch of stable HCs are obtained with no evidence of oscillations. In Fig. 3(a) we show the branches of different solutions in a $2C$ scan where the intensity of the HSS is kept constant at the value 1 by changing the pump P as shown in Fig. 3(b). The relation between P and $2C$ is basically linear for a wide range of parameter values. Fig. 3(c) instead shows them in P^2 scan where the fixed value of $2C = 30$ is used. Other than the stable and oscillating HC patterns depicted in Fig. 3(a), stable roll and bistable roll-honeycomb patterns can also be obtained in this scan in the absence of CS solutions. Examples of these pattern solutions and DCSs are shown in Fig. 4.

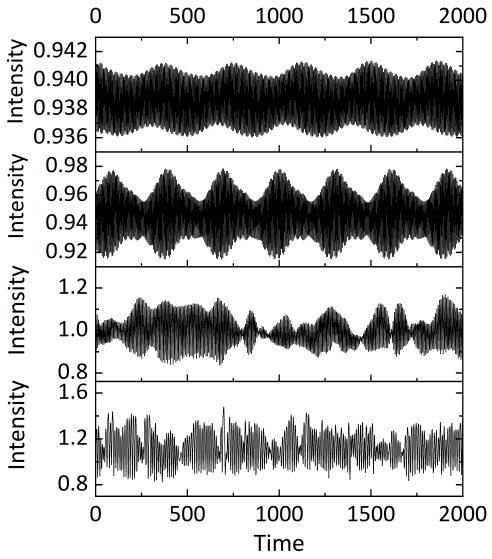

FIG. 5. Time evolution of the intensity in an arbitrary point of the HC pattern for different control parameter values. From top to bottom: $2C = 32.25$, $P^2 = 8.17$; $2C = 32.50$, $P^2 = 8.24$; $2C = 34.00$, $P^2 = 8.65$; and $2C = 35.15$, $P^2 = 8.98$. Other parameter values in Fig. 2.

III. OSCILLATING AND CHAOTIC HONEYCOMBS

Adiabatic scans reveal a wide range of $2C$ values leading to pattern solutions extending from $2C = 18.8$ up to 35.15 (see upper curve in Fig. 3(a)). This is due to a secondary bifurcation point from stable HCs to oscillating HCs. As depicted in Fig. 3(a), part of the branch that corresponds to oscillating HCs in an adiabatic scan is bistable with homogeneous solutions. The interval begins at $2C = 31.25$ and ends at 32.82. This implies that one can excite oscillating HCs from a homogeneous background by transient switching pulses of an appropriate width.

Fig. 5 displays the intensity time trace of an arbitrary point on the HC pattern for different values of the control parameters $2C$ and P^2. Fig. 6 displays the corresponding trajectories in an intensity-phase plot and their power spectra. Transition to chaos is evident starting from a limit cycle around an unstable fixed point and then its break up displayed in Fig. 6(a) to Fig. 6(d) when increasing the control parameter value from $2C = 32.25$ to 35.15. This is consistent with the changes taking place in the power spectra from Fig. 6(e) to Fig. 6(h). Transition to chaos is better understood by noting that the number of frequency components included in the oscillations evolves from two frequencies around 0.17 and 0.34 to many

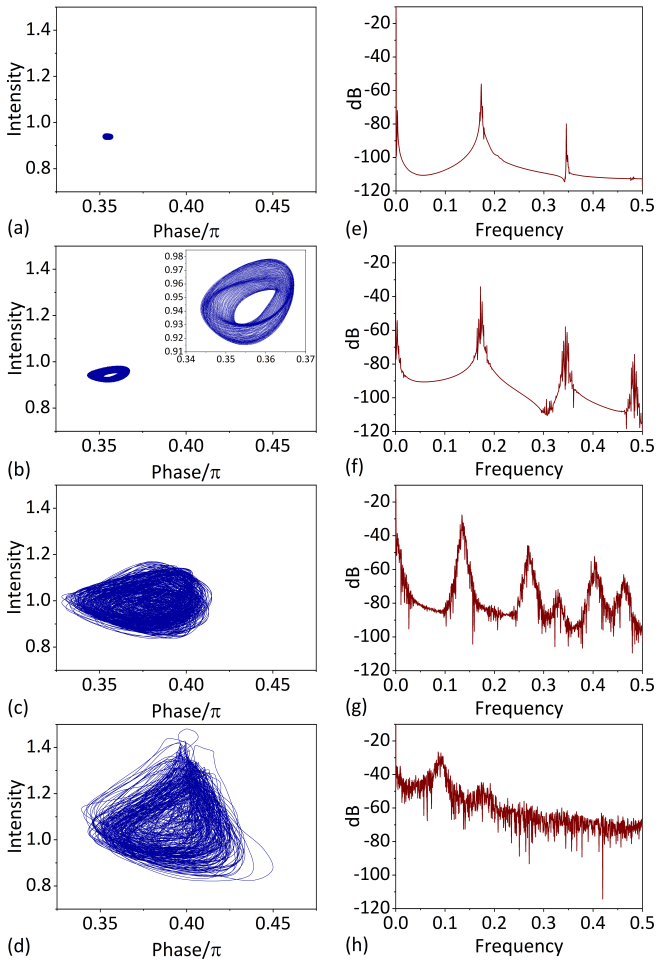

FIG. 6. Trajectories in the intensity-phase sub-space for Fig. 5 (a-d) and their power spectra (e-h).

components around these two central peaks. This appears to be the typical scenario of the quasi-periodic route to chaos [58].

IV. OSCILLATING DARK CAVITY SOLITONS AND THEIR INTERACTION

By injecting a transient pulse into the cavity in the bistable region and with the appropriate phase a DCS of the kind seen in Fig. 4(d) can be excited. Depending on the value of the control parameters, the excited DCS may oscillate in time and in a variety of fashions. The range of $2C$ values supporting oscillating DCSs is from 32.15 to 32.82. Dynamical behavior of DCSs for different values of the control parameters is shown in Fig. 7 where time traces of the intensity in the centre of the DCS are presented. Here, the value of $2C$ is decreased from top to bottom to illustrate the change in the dynamics. Uniform oscillations of the DCS

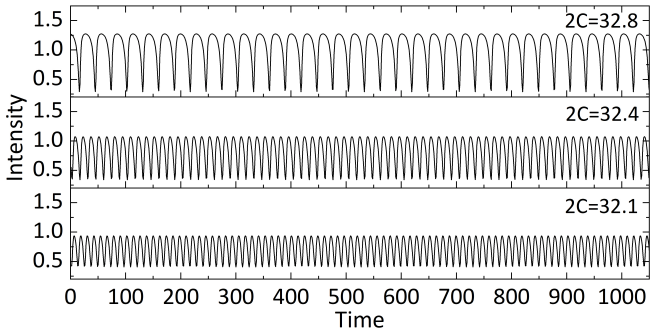

FIG. 7. DCS intensity versus time for $2C = 32.8$, $P^2 = 8.32$; $2C = 32.4$, $P^2 = 8.21$; and $2C = 32.1$, $P^2 = 8.13$ from top to bottom.

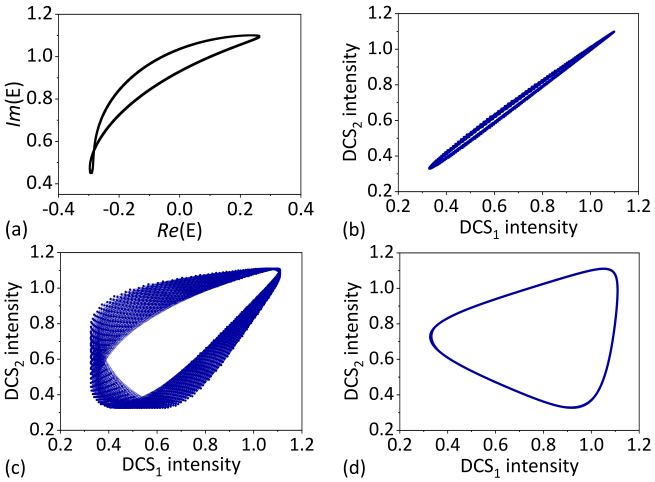

FIG. 8. (a) The complex plane orbit for a single oscillating DCS at the same parameter values corresponding to the top row of Fig. 7. **(b)-(d)** Intensity variations of the two interacting DCSs with respect to each other at different separation distances: (b) d=w/6, (c) w/4, and (d) d=w/1.5. Parameter values are: $2C = 32.5$ and $P^2 = 8.24$.

intensity are observed with decreasing amplitude and increasing frequency when reducing the parameter $2C$. An example trajectory for a single DCS in the Argand plane is depicted in Fig. 8(a).

Depending on the distance between two oscillating DCSs, different degrees of mutual correlation and coherence are possible. In Fig. 8(b-d), we show the intensities of two interacting oscillating DCSs plotted versus each other for different separation distances d. It is clearly seen that by increasing the separation distance, from (b) to (d) in Fig. 8, the DCSs move from full correlation at the minimum possible separation distance, d=w/6, to

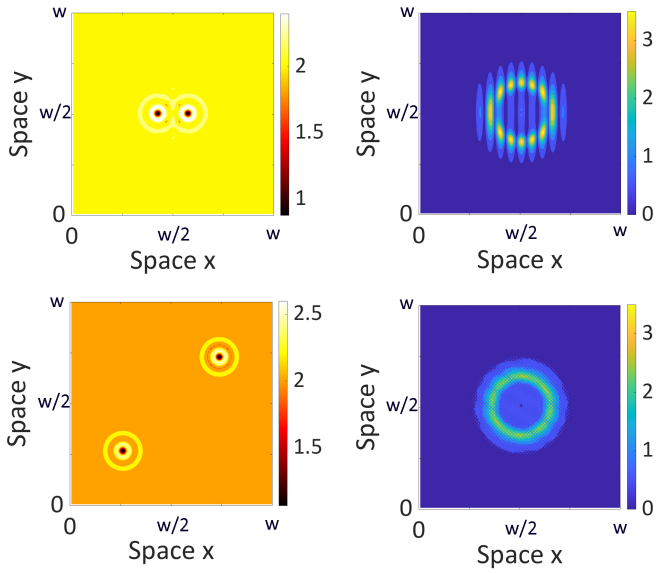

FIG. 9. Left panels: time-average of near-field intensity output profile for d=w/6 and w/1.5 respectively from top to bottom. Right panels: time-average of the associated far-field profiles: interferogram presents no fringes for d=w/1.5 (the picture at the bottom right) indicating the absence of mutual coherence between far located DCSs. Parameter values the same as in Fig. 8.

lack of correlation at a larger separation distance, for example d=w/1.5. Phase relationship between the interacting oscillating DCSs can be detected in the far field via an interference pattern which allows for measuring the spatial coherence of the binary structure. We show these interference patterns in Fig. 9 for the same mutually interacting DCSs and separation distances in Fig. 8. The two oscillating DCSs turn into coherent sources of radiation when the separation distance between them is small enough for complete (or partial) correlation. On the other hand, for large separation distances for which the two DCSs are uncorrelated the interference pattern fades away as it happens for two incoherent sources.

V. STATIC MULTIHEAD DUAL CHIMERA STATES

Almost two decades after the discovery of the so-called chimera states that started with mainly mathematical models, their extension to physical systems has been limited, see [59–61]. Chimera states are spatiotemporal patterns in which a system of identical oscillators is split into coexisting regions of coherent and incoherent oscillations. For a long time, research on these states were restricted to either phase oscillators or to the cases of weak coupling for

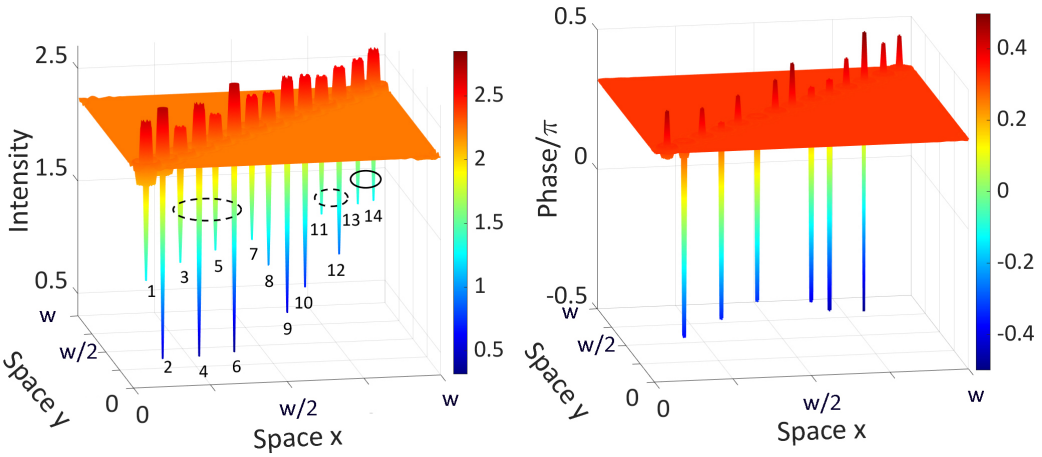

FIG. 10. 3D snapshot of the output in intensity (left) and phase (right) for the diagonal stripe of interacting oscillating DCSs. Anti-phase and in-phase locked DCSs are circled by dashed and solid lines respectively. The separation distance between DCSs is w/12. The control parameter values are $2C = 32.8$, $P^2 = 8.32$.

which approximations to phase oscillators is possible. In later studies where phase reduction was not used, the amplitudes of the individual oscillators vary only slightly around their average value and thus the analysis was still limited to the weak coupling case, see [48] for a comprehensive review. When these states were reported in regimes of strong coupling, the name amplitude-mediated chimera was adopted [62] and later studies showed that they survive small diffusion and can be extended to two-dimensional cases [63]. Due to the wide variety of chimeric features, researchers have tried several classification schemes based on, for example, the type of coupling and geometry [47, 64], spatial and temporal coherence [65], number of coherent and incoherent clusters [66, 67], and their dynamical behavior [51, 68–70]. Here we report the first observation of a collective behavior corresponding to coexistent regions of spatial and temporal coherence and incoherence in the output of a nonlinear cavity hosting interacting oscillating DCSs and try to illustrate their exotic properties along the lines of the aforementioned classifications.

To begin with, we simulate a diagonal stripe of length w/0.8 containing 14 oscillating DCSs with equal separation distance of w/12 (the minimum available to guarantee a full correlation), as shown in Fig. 10. The DCSs are switched simultaneously using intense transient Gaussian pulses of equal amplitudes (= 20) and widths (= $w/42$). The scenario is no different for even longer stripes containing more interacting DCSs as we shall see later.

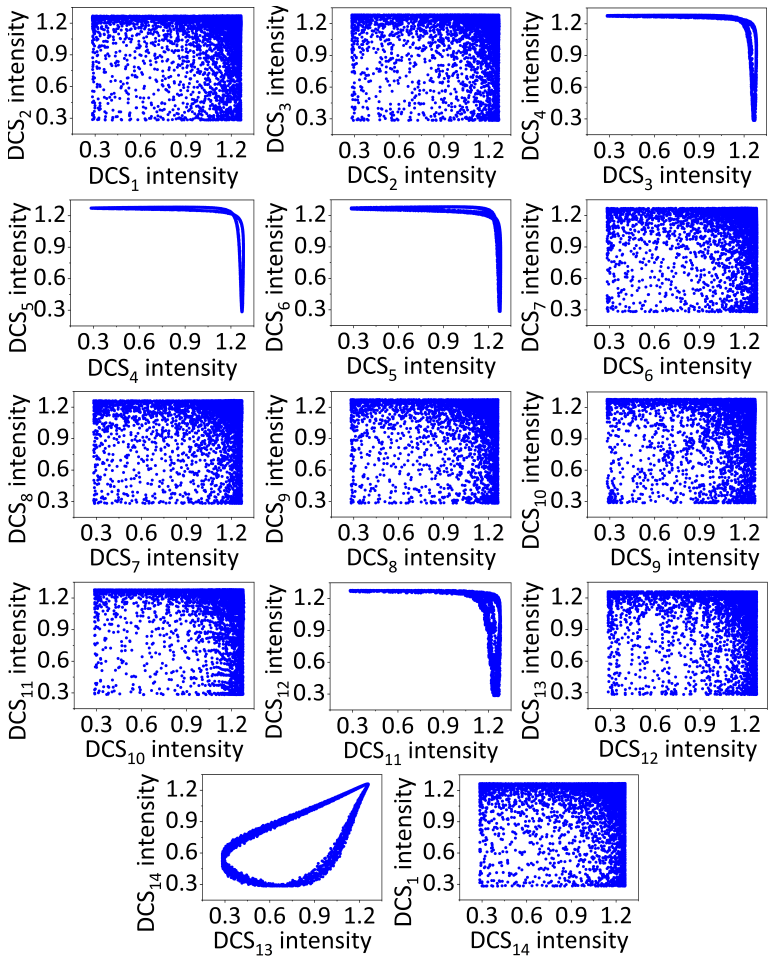

FIG. 11. Intensity values of the interacting oscillating DCSs in the diagonal stripe of Fig. 10. DCS_3 to DCS_6 and DCS_{11} to DCS_{12} experience anti-phase locking while in-phase locking occurs for DCS_{13} and DCS_{14}. The remaining DCSs form turbulent regions and separate the locked areas.

We aim to exhibit the formation of a static multihead dual chimera state: 'static' since the coherent and incoherent regions do not move along the stripe of DCSs, i.e. the DCSs that adopt correlated (or uncorrelated) oscillations in the stripe keep the same dynamics over time [65], 'multihead' due to the presence of several incoherent regions (heads) which separate the coherent areas [71, 72], and 'dual' signalling coexisting regions of in-phase and anti-phase synchrony [51]. We note that the background away from the tails of the DCSs has fixed intensity and phase values in time.

Despite having a large amplitude of oscillations, DCSs in our chimera (no matter if they are in phase, or out-of-phase, or independent) follow the same trajectory in the complex plane of individual (uncoupled) DCS as shown in Fig. 8(a) implying a regime of weak

coupling. This is unique compared to previously reported chimera states with relatively weak coupling but with amplitudes of individual oscillators deviating only a few percent from their average values [48, 73]. In Fig. 11 we show the mutual interaction of oscillating DCSs in the diagonal stripe in terms of their intensities plotted against each other while evolving in time. This leads to the formation of multiple anti-phase and in-phase coherent regions (circled by dashed and solid lines, respectively, in Fig. 10) separated by areas where the DCS oscillate incoherently with each other (corresponding to the panels in Fig. 11 with scattered dots).

We further check the robustness of these results about chimera states by simulating stripes containing more interacting oscillating DCSs in horizontal and vertical lines, instead of diagonal lines, and in simulations with 512×512 grid points. In Fig. 12 and 13, we show snapshots at fixed time intervals separated by the oscillation period of the locked DCSs. Domains of in-phase and anti-phase synchrony are clearly distinguishable by the fixed phase values of the respective DCS (see panels (a),(c), and (e) in Fig. 12 and Fig. 13) and the unlocked regions are evident by their scattered values in these sequential snapshots.

Finally we have checked that chimeras with static regions of correlated and uncorrelated oscillations of DCSs survive when expanding the stripes in a direction perpendicular to the stripe itself. These correspond to two dimensional chimera states. The results are shown in Fig. 14 in terms of phase plots in three sequences separated by the oscillation period of DCSs. In-phase coherent DCSs are inside solid boxes and those of anti-phase inside dashed boxes in these phase plots. Their intensities are shown in Fig. 15 (b) and (c) along with an example of uncorrelated oscillations in Fig. 15 (a) corresponding to the first and second DCSs in the same line.

VI. CONCLUSION

By considering a three-level medium displaying EIT in a cavity under the action of a transversally extended pump, the transition from homogeneous states to stationary and oscillating HC structures has been investigated. By increasing the value of the control parameters, stationary HC patterns start to oscillate first periodically and then chaotically through a quasi-periodic rout to chaos. Dark cavity solitons are also shown to reach a

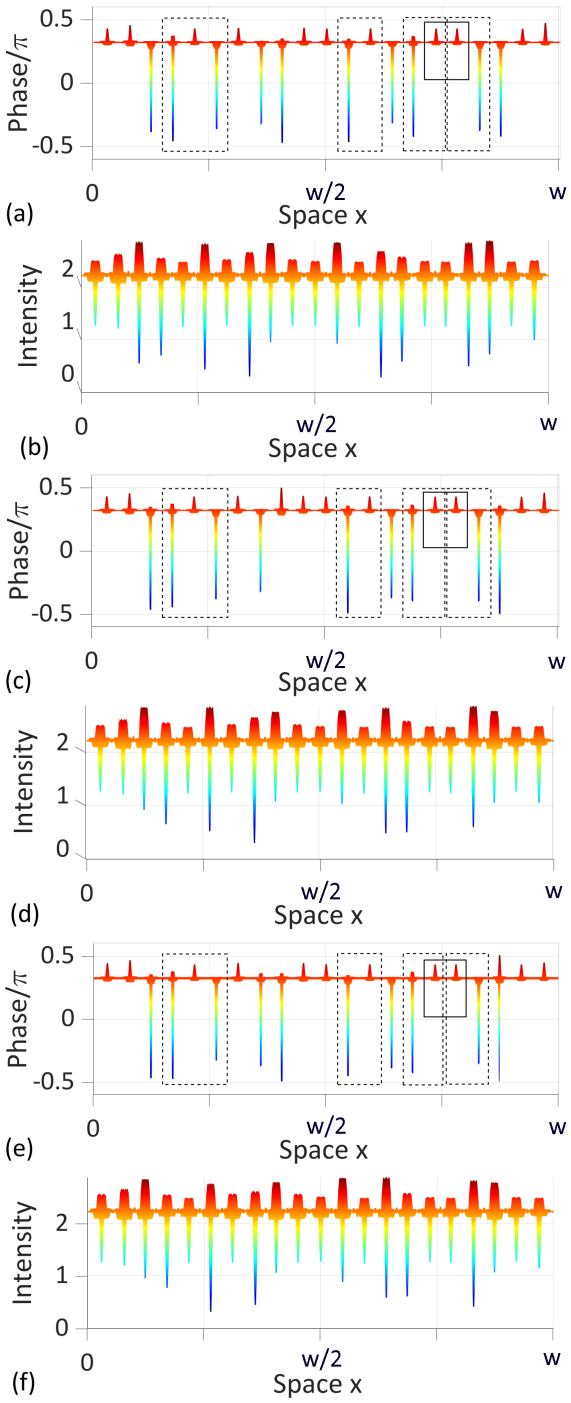

FIG. 12. Horizontal stripe of 21 coupled oscillating DCSs featuring both in-phase and anti-phase lockings coexisting with unlocked DCSs. (a,b), (c,d), and (e,f) are the phase and intensity plots at fixed time intervals equal to 28 time units respectively. In-phase coherent DCSs are inside solid boxes and those of anti-phase DCSs inside dashed boxes in the phase plots. The remaining DCSs are unlocked. Parameter values are the same as in Fig. 10.

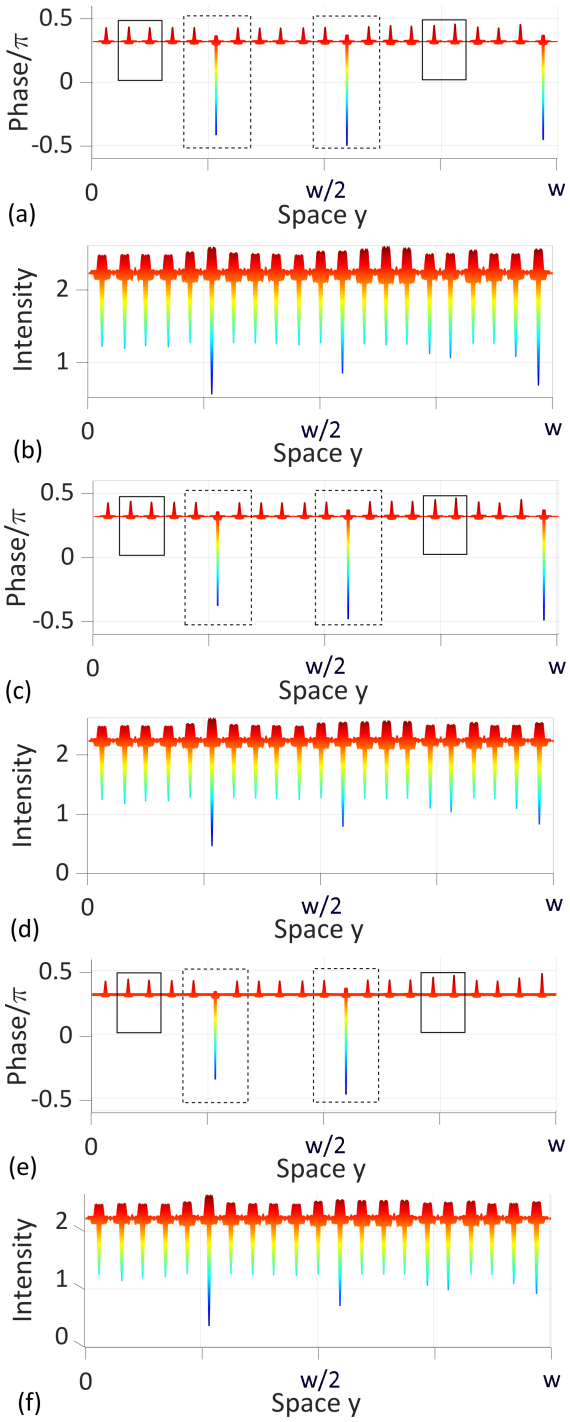

FIG. 13. Vertical stripe of 21 coupled oscillating DCSs featuring both in-phase and anti-phase lockings coexisting with unlocked DCSs. (a,b), (c,d), and (e,f) are the phase and intensity plots at fixed time intervals equal to 28 time units respectively. In-phase coherent DCSs are marked with solid boxes and those of anti-phase DCSs with dashed boxes in phase plots. The remaining DCSs are unlocked. Parameter values are the same as in Fig. 10.

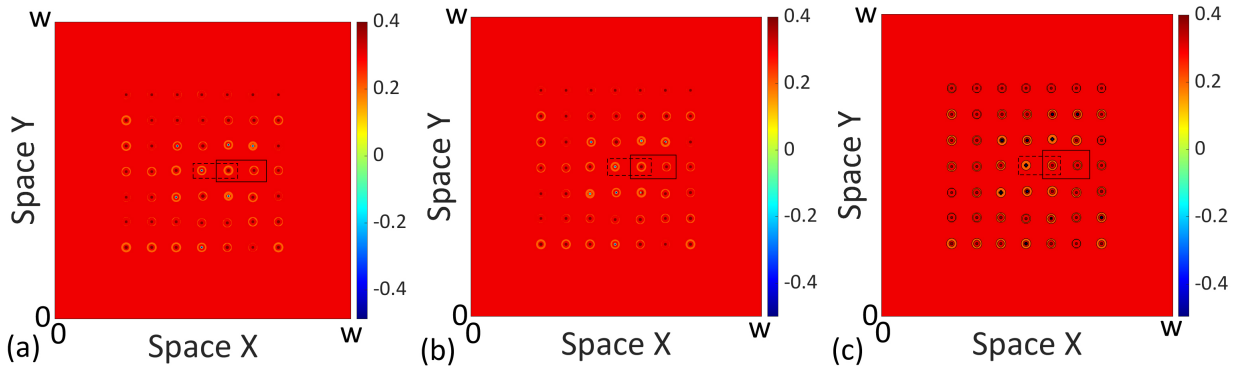

FIG. 14. **Mansour, is the phase/pi plotted here? If so, you need to say that. Please change the scale of phase/pi from -0.45 to 0.4, to -0.6 to 0.6 as in Fig.13 so that there will be much less blinding red in the snapshots. Update the caption (note that the time separation between (a)-(b)-(c) are not given) and write this in the reply to the referee. Thanks.** Temporal snapshots of two dimensional chimera states of DCSs. On the middle horizontal line, in-phase DCSs are inside solid boxes and those of anti-phase oscillations inside dashed boxes. The remaining DCSs in the line are unlocked. Parameter values are the same as in Fig. 10

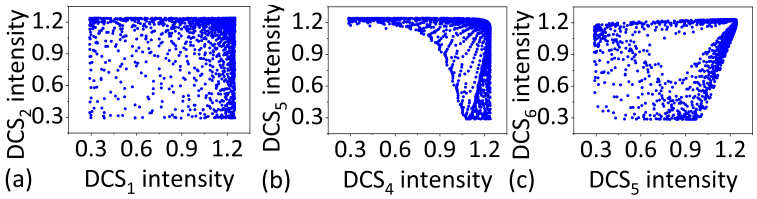

FIG. 15. Intensity values of the interacting oscillating DCSs in the middle horizontal line of 2D chimera of Fig. 14. (a) The intensity of DCS_2 versus that of DCS_1 shows uncorrelated oscillations, (b) the intensity of DCS_5 versus that of DCS_4 shows anti-phase oscillations and (c) the intensity of DCS_6 versus that of DCS_5 shows in-phase coherent oscillations. Parameter values are the same as in Fig. 10

regime of multi-frequency oscillations by changing the control parameter values. Mutual interaction of two oscillating dark cavity solitons results in different correlated and uncorrelated oscillations in their intensity and phase depending on their separation distances. Small separation distances correspond to strong coupling and coherence of the oscillations. Oscillation coherence is lost at large distances of the dark cavity solitons.

In arrays of equally spaced oscillating dark cavity solitons novel chimera states formed by in-phase and out-of-phase regions have been found in our nonlinear optical system. We showed that chains of coupled dark cavity solitons, identical in principle, can form coexisting stationary regions of in-phase and anti-phase coherence along with incoherent oscillations. These chimera states fall into the category of static multihead dual chimera states [48]. Here, symmetry breaking in the dynamics of the coupled DCSs is not due to background inhomogeneities and occurs in different spatial regions depending on the initial condition. Yet, once settled, the chimera state is stable with regions of coherent (synchronous) coupling and regions with incoherent coupling remaining unaltered in size and position in the long term. Chimera states are robust and survive in fully two dimensional regions of dark cavity solitons on a square grid. We believe that this complex behavior can be attained in experimental realizations of EIT media in optical cavities where they can shed light on fundamental aspects of collective behavior in complex systems. **Although Eq. 1 contains some standard approximations, the results of this work can find general application in a variety of nonlinear devices displaying EIT such as pilydimethyl-siloxane-coated silica resonators [74], microtoroids coupled with microspheres [75] and cavities containing Rubidium gases [76]. Moreover, EIT induced chimeras as presented here are expected in the presence of dispersion instead of diffraction [34] and in media with V or ladder energy level configurations.**

---

[1] M. C. Cross and P. C. Hohenberg, Rev. Mod. Phys. **65**, 851 (1993).

[2] M. C. Cross and H. Greenside, *Pattern Formation and Dynamics in Nonequilibrium Systems*, (Cambridge University Press, Cambridge, 2009)

[3] R. C. Desai and R. Kapral, *Dynamics of Self-Organized and Self-Assembled Structures*, (Cambridge University Press, Cambridge, 2009)

[4] K. Staliunas and V. J. Sanchez-Morcillo, *Transverse Patterns in Nonlinear Optical Resonators*, (Springer-Verlag, Berlin, 2003).

[5] L. A. Lugiato, F. Prati and M. Brambilla, *Nonlinear Optical Systems*, (Cambridge University Press, Cambridge, 2015)

[6] L. Columbo, F. Prati, M. Brambilla, and T. Maggipinto , Eur. Phys. J. D **59**, 115 (2010).

[7] M. Turconi, F. Prati, S. Barland, and G. Tissoni, Phy. Rev. A **92**, 053855 (2015).

[8] D. Gomila, M. A. Matias, and P. Colet, Phy. Rev. Lett. **94**, 063905 (2005).

[9] A. Jacobo, D. Gomila, M. A. Matias, and P. Colet, Phy. Rev. A **78**, 053821 (2008).

[10] M. Eslami, M. Khanmohammadi, R. Kheradmand, and G.-L. Oppo, Phys. Rev. A **96**, 033836 (2017).

[11] G.-L. Oppo, A. M. Yao, D. Cuozzo, Phys. Rev. A **88**, 043813 (2013).

[12] C. J. Gibson, A. M. Yao, G.-L. Oppo, Phys. Rev. Lett. **116**, 043903 (2016).

[13] S. Coulibaly, M. Taki, A. Bendahmane, G. Millot, B. Kibler, and M. G. Clerc, Phys. Rev. X **9**, 011054 (2019).

[14] C. Rimoldi, S. Barland, F. Prati, G. Tissoni, Phys. Rev. A **95**, 023841 (2017).

[15] K. Talouneh, C. Rimoldi, R. Kheradmand, G. Tissoni, M. Eslami, Phys. Rev. A **102**, 033508 (2020).

[16] K. Talouneh, R. Kheradmand, G. Tissoni, M. Eslami, Phys. Rev. A **105**, 013501 (2022).

[17] C. Rimoldi, M. Eslami, F. Prati, and G. Tissoni , Phys. Rev. A **105**, 023525 (2022).

[18] D. Gomila and P. Colet, Phys. Rev. E **66**, 046223 (2002).

[19] D. Gomila and P. Colet, Phys. Rev. A **68**, 011801 (2003).

[20] D. Gomila, T. Ackemann, E. G. Westhoff, P. Colet, and W. Lange , Phys. Rev. E **69**, 036205 (2004).

[21] T. Ackemann, W. Firth, and G.-L Oppo , Fundamentals and Applications of Spatial Dissipative Solitons in Photonic Devices, Adv. At. Mol. Opt. Phys. **57**, 323 (2009).

[22] S. Barland, J. R. Tredicce, M. Brambilla, L. A. Lugiato, S. Balle, M. Giudici, T. Maggipinto, L. Spinelli, G. Tissoni, T. Knoedl, M. Miller, and R. Jager, Nature **419**, 699 (2002).

[23] F. Pedaci, S. Barland, E. Caboche, P. Genevet, M. Giudici, J. R. Tredicce, T. Ackemann, A. J. Scroggie, W. J. Firth, G.-L. Oppo, G. Tissoni, and R. Jager, App. Phys. Lett. **92**, 011101 (2008).

[24] M. Eslami, and R. Kheradmand, Opt. Rev. **19**, 242 (2012).

[25] A. Jacobo, D. Gomila, M. A. Matias, P. Colet, New J. of Phys. **14**, 013040 (2012).

[26] M. Eslami, R. Kheradmand, F. Prati, Phys. Rev. A **89**, 013818 (2014).

[27] M. Eslami, R. Kheradmand, J. of Mod. Opt. **61**, 116 (2014).

[28] M. Eslami, S. Z. Gandomani, F. Prati, H. Tajalli, R. Kheradmand, J. of Opt. **19**, 015502 (2016).

[29] M. Eslami, N. H. Khiavi, R. Kheradmand, F. Prati, Phys. Rev. A **98**, 043807 (2018).

[30] S. R. Anbardan, M. Eslami, R. Kheradmand, F. Prati, J. of Opt. **21**, 125405 (2019).

[31] S. R. Anbardan, M. Eslami, R. Kheradmand, Opt. Commun. **474**, 126093 (2020).

[32] T. J. Kippenberg, A. L. Gaeta, M. Lipson, and M. L. Gorodetsky, Science **361**, 567 (2018).

[33] H. Bao, A. Cooper, M. Rowley, L. Di Lauro, J. S. Totero Gongora, S. T. Chu, B. E. Little, G.-L. Oppo, R. Morandotti, D. J. Moss, B. Wetzel, M. Peccianti, and A. Pasquazi, Nat. Phot. **13**, 384 (2019).

[34] G.-L. Oppo, D. Grant, and M. Eslami, Phys. Rev. A **105**, L011501 (2022).

[35] A. Scroggie, W. Firth, G. McDonald, M. Tlidi, R. Lefever, and L. Lugiato, Chaos, Solitons and Fractals **4**, 1323 (1994).

[36] W. Firth, G. Harkness, A. Lord, J. McSloy, D. Gomila, and P. Colet, J. Opt. Soc. Am. B **19**, 747 (2002).

[37] D. Turaev, A. Vladimirov, and S. Zelik, Phys. Rev. Lett. **108**, 263906 (2012).

[38] T. Elsass, K. Gauthron, G. Beaudoin, I. Sagnes, R. Kuszelewicz, and S. Barbay, Eur. Phys. J. D **59**, 91 (2010).

[39] F. Leo, L. Gelens, P. Emplit, M. Haelterman, and S. Coen, Opt. Express **21**, 9180 (2013).

[40] K. Panajotov and M. Tlidi, Opt. Lett. **39**, 4739 (2014).

[41] M. Eslami and G.-L. Oppo, The Euro. Phys. J. D **75**, 1 (2021).

[42] P. Genevet, M. Turconi, S. Barlanda, M. Giudici, and J.R. Tredicce, Eur. Phys. J. D **59**, 109 (2010).

[43] H. Vahed, R. Kheradmand, H. Tajalli, G. Tissoni, L. A. Lugiato, and F. Prati, Phys. Rev. A **84**, 063814 (2011).

[44] A. Pikovsky, M. Rosenblum and J. Kurths, Synchronization: A universal concept in nonlinear sciences, Cambridge University Press, (2001).

[45] Y. Kuramoto and D Battogtokh, Nonlinear Phenom. Complex Syst. **5**, 380 (2002).

[46] D. M. Abrams and S. H. Strogatz, Phys. Rev. Lett. **93**, 174102 (2004).

[47] M. J. Panaggio and D. M. Abrams, Nonlinearity **28**, R67 (2015).

[48] S. W. Haugland, J. Phys. Complex. **2**, 032001 (2021).

[49] Z. Faghani, Z. Arab, F. Parastesh, S. Jafari, M. Perc, M. Slavinec, Chaos, Solitons and Fractals **114**, 306 (2018).

[50] A. M. Cabanas, J. A. Vélez, L. M. Pérez, P. Diaz, M. G. Clerc, D. Laroze, B. A. Malomed, Chaos, Solitons and Fractals **146**, 110880 (2021) .

[51] G. Petrungaro, K. Uriu, and L. G. Morelli, Phys. Rev. E **96**, 062210 (2017).

[52] G.-L. Oppo, Journal of Modern Optics, **57**, 1408 (2010).

[53] M. Eslami, R. Kheradmand, D. McArthur, and G.-L. Oppo, Phy. Rev. A **90**, 023840 (2014).

[54] M. Eslami, R. Kheradmand, and G.-L. Oppo, J. of Phy. B: Atom., Mol. and Opt. Phys. **53**, 075402 (2020).

[55] L. A. Lugiato and R. Levefer, Phys. Rev. Lett. **58**, 2209 (1987).

[56] L. A. Lugiato and C. Oldano, Phys. Rev. A **37**, 3896 (1988).

[57] G.-L. Oppo, J. Math. Chem. **45**, 95–112 (2009).

[58] T. Kapitaniak, Chaos for Engineers, Springer Berlin, Heidelberg (2000).

[59] A. M. Hagerstrom, T. E. Murphy, R. Roy, P. Hövel, I Omelchenko, and E Schöll, Nat. Phys. **8**, 658 (2012).

[60] F. Bohm, A. Zakharova, E. Scholl, and K. Ludge, Phys. Rev. E **91**, 040901(R) (2015).

[61] J. Shena, J. Hizanidis, V. Kovanis, and G. P. Tsironis, Sci. Rep. **7**, 42116 (2017).

[62] G. C. Sethia, A. Sen, and G. L. Johnston, Phys. Rev. E **88**, 042917 (2013).

[63] L. Schmidt, K. Schonleber, K. Krischer, and V. Garcia-Morales, chaos **24**, 013102 (2014).

[64] O. E. Omelchenko, Nonlinearity **31**, R121 (2018).

[65] F. P. Kemeth, S. W. Haugland, L. Schmidt, I. G. Kevrekidis, and K. Krischer, Chaos **26**, 094815 (2016).

[66] G. C. Sethia, A. Sen, and F. M. Atay, Phys. Rev. Lett. **100**, 144102 (2008).

[67] I. Omelchenko, O. E. Omelchenko, P. Hovel, and E. Scholl, Phys. Rev. Lett. **110**, 224101 (2013).

[68] R. Ma, J. Wang, and Z. Liu, Europhys. Lett. **91**, 40006 (2010).

[69] G. Bordyugov, A. Pikovsky, and M. Rosenblum, Phys. Rev. E **82**, 035205 (2010).

[70] S. Olmi, E. A. Martens, S. Thutupalli, and A. Torcini, Phys. Rev. E **92**, 030901 (2015).

[71] Y. L. Maistrenko, A. Vasylenko, O. Sudakov, R. Levchenko, and V. L. Maistrenko, Int. J. Bifurcation Chaos **24**, 1440014 (2014).

[72] L. Larger, B. Penkovsky, and Y. Maistrenko, Nat. Commun. **6**, 7752 (2015).

[73] C. R. Laing, Phys. Rev. E **81**, 066221 (2010).

[74] H. Qin, M. Ding, and Y. Yin, Adv. Photonics Res. **1**, 2000009 (2020).

[75] T. Wang, Y.-Q. Hu, C.-G. DU, and G.-L. Long, Opt. Express **27**, 7344 (2019).

[76] A. Joshi, A. Brown, H. Wang, and M. Xiao, Phys. Rev. A **67**, 041801(R) (2003).